REPORT DOCUMENTATION PAGE

Form Approved
OMB No. 0704-0188

1. AGENCY USE ONLY *(Leave blank)*	2. REPORT DATE	3. REPORT TYPE AND DATES COVERED
	August 1992	Technical Paper

4. TITLE AND SUBTITLE
Two-Dimensional Aerodynamic Characteristics of Several Polygon-Shaped Cross-Sectional Models Applicable to Helicopter Fuselages

5. FUNDING NUMBERS
WU 505-59-36-01

PR1L236003D313

6. AUTHOR(S)
Henry L. Kelley, Cynthia A. Crowell, and John C. Wilson

7. PERFORMING ORGANIZATION NAME(S) AND ADDRESS(ES)
Aeroflightdynamics Directorate
JRPO—Langley
Langley Research Center
Hampton, VA 23681

8. PERFORMING ORGANIZATION REPORT NUMBER
L-16951

9. SPONSORING/MONITORING AGENCY NAME(S) AND ADDRESS(ES)
National Aeronautics and Space Administration
Washington, DC 20546-0001
and
U.S. Army Aviation Systems Command
St. Louis, MO 63120-1798

10. SPONSORING/MONITORING AGENCY REPORT NUMBER
NASA TP-3233

AVSCOM TR-92-B-002

11. SUPPLEMENTARY NOTES
Kelley and Wilson: Aeroflightdynamics Directorate, JRPO—Langley, Hampton, VA; Crowell: Now at U.S. Army Europe, Bad Schwalbach, Germany.

12a. DISTRIBUTION/AVAILABILITY STATEMENT
Unclassified–Unlimited

Subject Category 02

12b. DISTRIBUTION CODE

13. ABSTRACT *(Maximum 200 words)*
A wind-tunnel investigation was conducted to determine two-dimensional aerodynamic characteristics of nine polygon-shaped models applicable to helicopter fuselages. The models varied from 1/2 to 1/5 scale and were nominally triangular, diamond, and rectangular in shape. Side force and normal force were obtained at increments of angle of flow incidence from −45° to 90°. The data were compared with results from a baseline UH-60 tail-boom cross-sectional model. The results indicate that the overall shapes of the plots of normal force and side force were similar to the characteristic shape of the baseline data; however, there were important differences in magnitude. At a flow incidence of 0°, larger values of normal force for the polygon models indicate an increase in fuselage down load of 1 to 2.5 percent of main-rotor thrust compared with the baseline value. Also, potential was indicated among some of the configurations to produce high fuselage side forces and yawing moments compared with the baseline model.

14. SUBJECT TERMS	15. NUMBER OF PAGES
Helicopter; Fuselage; Tail boom; Blunt bodies; Aerodynamics	28
	16. PRICE CODE A03

17. SECURITY CLASSIFICATION OF REPORT	18. SECURITY CLASSIFICATION OF THIS PAGE	19. SECURITY CLASSIFICATION OF ABSTRACT	20. LIMITATION OF ABSTRACT
Unclassified	Unclassified		

Summary

An investigation was conducted in the Langley 14- by 22-Foot Subsonic Tunnel to determine two-dimensional aerodynamic characteristics of nine polygon-shaped models applicable to helicopter fuselages. The models varied from 1/2 to 1/5 scale and were nominally triangular, diamond, and rectangular in cross-sectional shape. Section side-force coefficients c_y and section normal-force coefficients c_z were obtained at a dynamic pressure of 20 psf and at incremental angles of flow incidence ϕ from $-45°$ to $90°$. The data were compared with results from a study of a UH-60 tail-boom cross-sectional model that served as the baseline configuration. Data from a UH-1 class helicopter were used in calculations to estimate effects of the cross-sectional aerodynamics on tail-rotor power.

The overall shapes of the plots of c_z and c_y versus ϕ for the polygon-shaped models were similar to the characteristic shape of the baseline data; however, there were important differences in magnitude. At $\phi = 0°$, for example, larger maximum values of c_z for the polygonal models than for the baseline model resulted in a computed increase in fuselage download penalties of about 1 to 2.5 percent of main-rotor thrust. Three of the polygonal models had larger values of the slope of c_y versus ϕ than the baseline configuration had, an indication of potential among the polygonal configurations for producing higher fuselage side-force and yawing moments when the cross sections are incorporated into a helicopter design. Key parameters from the polygon-shaped-model data were compared with UH-60, AH-64, and UH-1 two-dimensional model data previously reported.

Introduction

Single-rotor helicopters are subject to complex airflows generated by the main- and tail-rotor wakes and the ambient wind. These airflows create aerodynamic forces on the fuselage and the tail-boom assembly which, during hover and low-speed sideward flight, must be counteracted by increased main-rotor and tail-rotor thrust to maintain aircraft trim (refs. 1 and 2). The additional thrust increases the power requirements, which results in a reduction in both payload and yaw control margins. The magnitude of the aerodynamic forces on the fuselage is influenced by the cross-sectional shape and size of the fuselage as well as by the angle of attack and dynamic pressure in the wake around the fuselage. To optimize the aerodynamics, a fuselage cross-sectional configuration should be shaped to minimize the down load on the fuselage, which must be offset by additional main-rotor thrust. Also, the side force on the boom should be in the same direction as tail-rotor thrust to help decrease the thrust. The steeper the slope of the fuselage side-force coefficient c_y/ϕ and the larger the positive and negative values of the section side-force coefficient c_y, the more sensitive the fuselage is to the velocity and angle-of-attack changes and the greater the potential is for fuselage yawing moments in crosswinds and sideward flight with the attendant burden on tail-rotor horsepower. The steepness of the slope of c_y/ϕ, much like the lift-curve slope for an airfoil, indicates a larger side force for a given angle of flow incidence ϕ as well as increased sensitivity to changes in ϕ or velocity.

Previous studies (refs. 3 to 7) have been made in an effort to understand and modify helicopter tail-boom aerodynamic forces. Both two-dimensional wind-tunnel model and flight investigations were conducted on OH-58, UH-1, AH-64, and UH-60 helicopter tail booms. The two-dimensional tail-boom cross-sectional shapes investigated in the tunnel were generally cylindrical or oval. However, radar detectability requirements of future military helicopters require a change from more traditional designs to low-radar-signature cross-sectional designs that are generally polygon shaped. The aerodynamic characteristics of the polygonal shapes have not been fully investigated, and data from wind-tunnel models are necessary to validate computational methods that will be used to predict aerodynamic effects on vehicle performance and handling qualities.

To provide these data, a wind-tunnel investigation was conducted in the Langley 14- by 22-Foot Subsonic Tunnel with nine two-dimensional polygon-shaped models that varied from 1/2 to 1/5 scale. The models, shown in figure 1, were based on design information from an investigation sponsored by the U.S. Army on fuselage low-radar cross sections and represent possible future fuselage cross sections. The results from the polygon-shaped models were compared with those of a modern U.S. Army utility helicopter tail-boom cross-sectional model (UH-60), which served as the baseline configuration (ref. 3). When calculations were made to determine the effect of side-force characteristics on tail-rotor power, a UH-1 class helicopter (Bell 204B) was used because of the type of flight data available. Aerodynamic forces were measured at a free-stream dynamic pressure q_∞ of 20 psf for angles of ϕ from $-45°$ to $90°$. The baseline configuration data were taken at $q_\infty = 25$ psf (ref. 3). The results are presented as the section normal-force coefficient c_z and c_y as a function of ϕ for each configuration and are compared with results from the baseline model tests. Calculations based on an assumed helicopter were made to obtain the

approximate effects of the variations in side-load and down-load section coefficients on tail-rotor and main-rotor power required compared with those of the baseline configurations.

Symbols

Conventions for positive sense of flow inclination, model reference dimensions, and aerodynamic coefficients are shown in figure 2.

b	maximum width of model, in.
c	maximum depth of model, in.
c_y	section side-force coefficient, $\frac{\text{Side force per unit length}}{bq_\infty}$
c_z	section normal-force coefficient, $\frac{\text{Longitudinal force per unit length}}{bq_\infty}$
PF_{tr}	power-factor ratio of tail-rotor power required to balance aerodynamic force of tail boom with polygonal cross sections to tail-rotor power required to balance aerodynamic force of baseline (Bell 204B) tail boom
q_∞	free-stream dynamic pressure, $\frac{1}{2}\rho V^2$, psf
R	Reynolds number, $\frac{\rho V c}{12\mu}$
r	corner radii of fuselage cross section, in.
$\frac{\Delta T_{\text{mr}}}{T_{\text{mr}}}$	change in main-rotor thrust required for helicopter with tail boom equipped with the polygon-shaped cross sections compared with helicopter with baseline (UH-60) tail boom
V_∞	free-stream velocity in tunnel, ft/sec
β	angle of sideslip, positive with relative wind approaching aircraft from the right, deg
μ	absolute viscosity, slug/ft-sec
ρ	free-stream air density, slug/ft^3
ϕ	angle of flow incidence in plane normal to axis of two-dimensional cylinder, deg

Abbreviations:

BL	baseline
TRDSC	tail-rotor drive-shaft cover
S_x	polygon-shaped-model identification, with x indicating configuration, $x = 1, 2, \ldots, 9$

Model and Apparatus

Nine polygon-shaped models representative of cross sections of rotorcraft fuselages or tail booms were tested. The models varied from approximately 1/2 to 1/5 scale. Dimensions and cross-sectional shapes of the nine models and of the baseline UH-60 tail-boom model are shown in figure 1. Model configurations S_1 and S_2 were both basically triangular, with rounded corners on the bottom. Configuration S_1 had a flat top and configuration S_2 had a rounded top that could serve as a tail-rotor drive-shaft cover (TRDSC). Configurations S_3 and S_4 were both diamond shaped, with a nearly flat bottom. Configuration S_4 had a pointed top and configuration S_3 had a small, flat top. Configurations S_5 and S_6 were truncated triangles. Configuration S_6 had a TRDSC shape on top of the truncation. Configurations S_7 and S_8 were both diamond shaped and looked similar to configuration S_3 except for larger flat tops. Configuration S_8 had a TRDSC shape on top. Configuration S_9 was basically a vertical rectangle with rounded corners and had a TRDSC shape on top. The baseline model section was taken from the tail boom of a UH-60 at a station approximately underneath the 80-percent-radius station of the main-rotor blade and was a rounded oval shape with a TRDSC on top.

The models were constructed of aluminum sheet metal attached to aluminum bulkheads with flush mounting screws. The surfaces were smooth without the protruding rivet heads characteristic of helicopter fuselages and tail booms. Configurations S_3, S_4, S_7, and S_8 were fabricated from wood and aluminum. The model reference dimensions and directions of aerodynamic coefficients are shown in figure 2.

The installation of one of the models in the 14- by 22-Foot Subsonic Tunnel is shown in figure 3. A technical description of the 14- by 22-Foot Subsonic Tunnel is given in reference 8. A schematic drawing of the components of the helicopter fuselage cross-sectional test apparatus is shown in figure 4. The test apparatus was constructed in three major sections. The upper and lower sections were rigidly mounted, whereas the middle section (metric section) was attached to a six-component strain-gage balance. The apparatus was rotated about the vertical axis to vary the angle of flow incidence ϕ on the model. Large circular plates (48 in. in diameter) were placed at both ends of the apparatus to ensure that evenly

distributed two-dimensional flow would occur on the metric section.

Test Procedures and Accuracy

Data were taken at a constant q_∞ as the model was rotated through the range of ϕ from $-45°$ to $90°$. Data were taken every $5°$ from $-25°$ to $30°$ and every $10°$ from $-45°$ to $-25°$ and from $30°$ to $90°$. These angles are equivalent to an angle of attack on the helicopter fuselage or tail boom due to main-rotor downwash and sideward flight airspeeds. The value $q_\infty = 20$ psf was selected to include the approximate Reynolds numbers experienced by full-scale helicopters ($1.0 \times 10^6 < R < 1.8 \times 10^6$). Free-stream dynamic pressure, as it relates to Reynolds number, is shown in figure 5 for the baseline model and the nine polygonal models.

During calibration with all beams fully loaded, the strain-gage balance used in the test apparatus for each of the models had an accuracy for both normal force and side force of ± 1.25 lb; however, the general repeatability of the force measurements was found to be approximately ± 0.20 lb. The balance had an accuracy at $q_\infty = 20$ psf of ± 0.003 for both normal-force coefficient and side-force coefficient, with a repeatability determined to be ± 0.001 for the coefficients.

Because the maximum test free-stream Mach number was 0.11, compressibility effects were negligible. Because of the small volume of the apparatus relative to the test-section volume, the data did not require correction for blockage effects (ref. 9).

Based on results in reference 3, several factors were considered that could have caused uncertainties in the data, such as model surface roughness, R, hysteresis effects caused by flow separation, and flow turbulence level in the test section. For the first factor, the model surface was not polished, but unlike typical helicopter fuselage surfaces it had no rows of rivet heads. The sheet metal was secured on the model frame by sunken screws. The screw holes were then taped over.

Regarding the second factor, lift and drag forces measured on the models are known to vary widely as a function of tunnel velocity, particularly in the critical R range. Full-scale rotorcraft experience varying values of R, and for $R = 0.3 \times 10^6$ to 0.7×10^6, large changes are known to occur in lift and drag on blunt bodies such as these. Because the data in this investigation were taken at $R = 1.0 \times 10^6$ to 1.8×10^6 (fig. 5), large changes in aerodynamic forces as a function of R were not a concern (refs. 10 and 11).

A third factor that can affect aerodynamic results as a function of angle of attack or airspeed is hysteresis caused by flow separation. This effect can influence the sequence used when q_∞ or ϕ are varied to take data points. To determine the effects of changing the sequence of ϕ at a given q_∞, several runs were made for $\phi = -45°$ to $90°$ and then for $\phi = 90°$ to $-45°$. The results indicated that there was relatively little difference in the data. Hysteresis in the data can also be experienced during a q_∞ sweep. If, for example, one run is taken with q_∞ increasing and the next taken with q_∞ decreasing, repeatability of the data may be poor. This effect was avoided by increasing tunnel q_∞ from 0 to 20 psf and then varying ϕ in increments consistently from $-45°$ to $90°$.

The final factor considered was turbulence in the tunnel test section. Because of recent improvements to the 14- by 22-Foot Subsonic Tunnel, the turbulence level was only 0.1 percent of free-stream velocity (ref. 8).

Presentation of Data

The results are presented as the section normal-force coefficient c_z and the section side-force coefficient c_y as a function of angle of flow incidence ϕ. Summary charts for the parameters c_y/ϕ and c_z at $\phi = 0°$ for configurations S_1 to S_9 and calculated effects of these parameters on tail-rotor and main-rotor power are also presented. The coefficients are based on the dimension b (maximum width of model), which is consistent with presentation of data in reference 3 and references 10 to 15. The baseline tail-boom cross-sectional data were obtained from reference 3.

The data are presented as follows:

Discussion of Results for General Aerodynamic Characteristics

The section side-force coefficient c_y and section normal-force coefficient c_z as a function of ϕ are presented and discussed. The data from the polygon-shaped sections are compared with data from the UH-60 baseline as well as with data from the other polygon models. Results from calculations based on these data are presented to show the effects of c_z and c_y on main-rotor and tail-rotor power relative to that of the baseline.

The relationship between ϕ and the sideward velocity of a helicopter in combination with downwash velocity from the main rotor can be expressed with simplifying assumptions as $\tan\phi$ = Sideward velocity/Average downwash velocity. If a UH-1–sized helicopter weighing 8000 lb and with a rotor 48 ft in diameter is assumed, the rotor disk loading is calculated to be about 4.4 lb/ft^2 in hover. A rule-of-thumb assumption is that, in hover, the average downwash dynamic pressure is equal to disk loading; therefore, the average downwash velocity is computed to be about 60 ft/sec. In left or right sideward flight then, $\tan\phi$ = Sideward velocity/60 ft/sec, and a sideward velocity of 35 knots yields an angle of flow incidence ϕ at the fuselage of 45°. The sideward-flight-speed envelope for many helicopters is 0 to 35 knots; therefore, if a large percentage of the operational time spent is assumed to be between 20 knots right and 20 knots left, then the speed range could be represented by an equivalent range of ϕ of −30° to 30°.

Configurations S_1 to S_9 Versus Baseline

A summary of c_z and c_y as a function of ϕ for configurations S_1 to S_9 and for the baseline is presented in figure 6. The results indicate a wide variation in c_z and c_y over the range of ϕ investigated. The variations were not unexpected, based on the diversity of blunt shapes under consideration. The larger the positive value of c_z, the higher the fuselage down-load penalty that must be compensated for by main-rotor thrust. Within $-15° < \phi < 15°$, c_z is higher for S_1 to S_9 than for the baseline. For comparison purposes, at $\phi = 0°$ a majority of the configurations (S_1 to S_8) result in values of c_z that are from 3.0 to 3.5 times larger than the baseline values. For S_9, c_z at $\phi = 0°$ is about twice as large as c_z at $\phi = 0°$ for the baseline.

Results of the data for c_y versus ϕ (fig. 6(b)) indicate a group of three configurations (S_1, S_2, and S_9) that have slopes (c_y/ϕ) which are steeper than the slope of the baseline data within the linear range $-10° < \phi < 10°$. Also for these configurations, the larger positive and negative values of c_y are about 2 times as large as the larger baseline values. The remaining configurations (S_3 to S_8) for $-10° < \phi < 10°$ have values of c_y/ϕ that vary from about one-third to one-eighth of the baseline value. Configuration S_3, which is a flat-bottom diamond with a blunt top, has a slope of c_y/ϕ of about one-seventh of the baseline value within $-10° < \phi < 10°$. More detailed comparisons of configurations S_1 to S_9 are presented in figures 7 to 13.

Configurations S_1, S_3, S_5, and S_7 Versus Baseline

Cross-sectional configurations S_1, S_3, S_5, and S_7 (polygonal shapes without a representative TRDSC) are compared with the baseline configuration in terms of c_z and c_y as a function of ϕ in figure 7. The configurations are representative of fuselage cross sections forward of a tail boom because no TRDSC is included in the shape.

Configurations S_1, S_3, S_5, and S_7 all have higher values of c_z for $-15° < \phi < 25°$ compared with the baseline values. This result is not unexpected because the baseline configuration has a smooth oval shape compared with the triangular- and diamond-shaped configurations without a TRDSC contour on top. Configuration S_3 has the highest value of c_z for $-30° < \phi < 25°$, with the c_z values of S_1, S_5, and S_7 being grouped together at $-10° < \phi < 10°$ but noticeably less (about 25 percent) at $\phi = 0°$ when compared with S_3. It is not obvious by visual inspection of the shapes of S_1, S_3, S_5, and S_7 why the values of c_z fall in this order.

At the more extreme values of ϕ investigated ($-45° < \phi < -20°$ and $25° < \phi < 90°$), values of c_z for the baseline configuration are within the range of the values of c_z for all the polygon-shaped configurations. Because the magnitude of fuselage down load is important in hover and low-speed flight (fuselage down-load loss varies between about 3 and 8 percent of total main-rotor thrust, depending on the particular helicopter design), the magnitude of c_z—

which depends on fuselage size and shape—must be given serious consideration by the designer. If a large percent of the low-speed operational time is assumed to be in the range of $-30° < \phi < 30°$ (between about 20 knots right and 20 knots left), the down-load penalty on a helicopter that uses S_1, S_3, S_5, and S_7 in the tail boom and fuselage would be expected to be appreciably higher compared with the penalty on one that uses fuselage sections shaped like the baseline configuration. In fact, if just the tail-boom portion of the fuselage is considered, and if it is assumed that the tail boom is responsible for one-fourth of the down-load penalty of a given helicopter fuselage that has a total fuselage down load of 4 percent of main-rotor thrust, then a tripling of the value of the baseline c_z at $\phi = 0°$ would result in a revised total fuselage down load of 6 percent, or a loss in overall vehicle lift capability of about 2 percent. Likewise, if the c_z were doubled compared with that of the baseline configuration, the loss in lift would be an additional 1 percent, for a total of 5 percent.

The linear portions of the curves of c_y versus ϕ in figure 7(b) are contained for the most part at $-10° < \phi < 10°$ and reflect attached flow (i.e., small degree of flow separation) on the models. The data at $\phi > 10°$ and $\phi < -10°$ represent conditions of massive flow separation (i.e., stall). At $-10° < \phi < 10°$, the steeper the slope of c_y/ϕ, the higher the potential side-force sensitivity for a given helicopter fuselage that incorporates these shapes in its design. Because these nine shapes are generally applicable to fuselage sections (both tail boom and sections forward of the tail boom), the effect of the steepness of c_y/ϕ on the net fuselage yawing moment would be an integrated effect along the entire fuselage length. Also, high fuselage side forces would result from large positive and negative values of c_y, and correcting for these forces requires some angle of bank to trim the vehicle when hovering over a spot on the ground in a crosswind.

The baseline configuration has a large value of c_y/ϕ when compared with those of other typical helicopter tail-boom cross-sectional configurations such as the UH-1 and the AH-64 (table I). Interestingly, S_1 (narrow truncated triangle shape) has a slope that is approximately 30 percent steeper than that of the baseline configuration for $-10° < \phi < 10°$, and the maximum positive and negative values for S_1 of c_y at $\phi = -20°$ and $\phi = 15°$, respectively, are about 2 times as large as the largest values of c_y for the baseline configuration. Also, c_y remains high for $15° < \phi < 90°$ and $-45° < \phi < -20°$ for S_1. The values of c_y/ϕ at $-10° < \phi < 10°$ for configurations S_3, S_5, and S_7 are about 13 percent, 38 percent, and 24 percent of the baseline c_y/ϕ, respectively. The value of the shallow slope of c_y/ϕ that is characteristic of the S_3 configuration (flat-bottom diamond with a blunt top) is similar to the value obtained on a two-dimensional circular cylinder reported in reference 3 (table I).

Configurations S_2, S_4, S_6, S_8, and S_9 Versus Baseline

Results from the polygon-shaped fuselage configurations equipped with representative TRDSC's (S_2, S_4, S_6, S_8, and S_9) are shown with those from the baseline configuration in figure 8. These configurations are geometrically similar to those considered in figure 7 except for the addition of the S_9 configuration (narrow rectangular shape with representative TRDSC). The variations of c_z and c_y with ϕ (fig. 8) are similar to the results shown in figure 7 and discussed in the previous section, with the addition of TRDSC's having a small effect on the overall results. The S_9 configuration produces c_z and c_y results that are expected based on results from S_2, which has a somewhat similar shape.

Figure 8(a) shows that the maximum c_z value at $\phi = 0°$ results from S_4. Also, the maximum value of c_z for S_4 is approximately the same as that for S_3 in figure 7(a). Within $-10° < \phi < 10°$, the value of c_z for the remaining configurations with TRDSC's fall above the baseline values.

The results shown in figure 8(b) are similar to those in figure 7(b), except that the addition of S_9 to the group results in values of c_y/ϕ and maximum positive and negative values of c_y on the order of those for S_1 and S_2. The comments given in the previous section regarding the results shown in figure 7(b) also generally apply to the results in figure 8(b).

Configurations With and Without a TRDSC

In this section of the paper, the effects on c_z and c_y of similarly shaped configurations with and without a TRDSC (S_1 and S_2, S_3 and S_4, S_5 and S_6, and S_7 and S_8) are discussed and compared with the effects of the baseline configuration. The results are presented in figures 9 to 12. The results for configuration S_9 alone are compared with the baseline in figure 13. Key values (c_z at $\phi = 0°$ and c_y/ϕ at $-10° < \phi < 10°$) taken from the data for configurations S_1 to S_9 are presented in table II. The same values for large-scale UH-60, UH-1, and AH-64 models taken from reference 3 are given in table I to provide additional comparisons. Data for these models were obtained in the same range of Reynolds

numbers as that for S_1 to S_9. The tail-boom sections (UH-1, UH-60, and AH-64) were modeled from a boom station under the 80-percent main-rotor-blade radial station.

S_1 versus S_2 versus baseline. The results for the narrow triangular configurations, one with a truncated top (S_1) and the second with a rounded top that modeled a TRDSC (S_2), are presented with the baseline results in figure 9. The results show a much larger c_z for S_1 and S_2 compared with that of the baseline for $-15° < \phi < 10°$ (fig. 9(a)). At $\phi = 0°$, c_z for S_1 and S_2 is about 3 times larger than the baseline c_z. Also, at $25° < \phi < 90°$, the values of c_z for S_1 and S_2 are lower than those for the baseline. The TRDSC on S_2 appears to have little effect in reducing c_z compared with S_1. The S_1 and S_2 shapes with higher values of c_z will yield larger down-load losses than will the baseline when incorporated into a helicopter fuselage.

Measurements in the linear portion of the curves in figure 9(b) ($-10° < \phi < 10°$) indicate that S_1 and S_2 have about 30 percent and 40 percent steeper slopes, respectively, than the baseline. The steepness of the slopes within this range of ϕ and the generally high values of c_y throughout the rest of the ϕ range indicate that, if these shapes were incorporated into a helicopter fuselage design, higher side-force and yawing-moment characteristics would likely result for S_1 and S_2 compared with the baseline. The effect of the TRDSC on S_2 compared with S_1 results in a steeper slope in the linear range and larger positive and negative values of c_y for ϕ beyond the linear range ($15° < \phi < -20°$).

S_3 versus S_4 versus baseline. Results for the S_3, S_4, and baseline configurations are presented in figure 10. The values of c_z at $-20° < \phi < 20°$ for S_3 and S_4 are much larger than the values for the baseline, and at $\phi = 0°$, the values for S_3 and S_4 are about 3.5 times larger than the baseline value (fig. 10(a)). In figure 10(b), slopes of c_y/ϕ within $-10° < \phi < 10°$ for S_3 and S_4 are low compared with c_y/ϕ of the baseline. The slope of c_y/ϕ for S_3 is the lowest of the nine polygon-shaped configurations investigated and, in fact, is nearly as low as c_y/ϕ for a circular cylinder reported in reference 3. (See tables I and II.) Within the same range of ϕ ($-10° < \phi < 10°$), S_4 has a value of c_y/ϕ about the same as that obtained on the two-dimensional AH-64 tail-boom model (cylindrical shape with a TRDSC) investigated in reference 3. (See tables I and II.) The TRDSC (pointed top) results in a steeper slope of c_y/ϕ for S_4 than for S_3 in the linear part of the curves. It has a negligible effect on c_z at $\phi = 0°$ and reduces c_z at $-35° < \phi < -10°$ and $15° < \phi < 35°$.

Outside the linear range of data points for $-10° > \phi > 10°$, the absolute values of c_y for S_3 and S_4 are generally lower than those for the baseline. If incorporated into a helicopter fuselage design, S_3 and S_4 would likely result in low fuselage side-force and yawing-moment characteristics compared with those of the UH-60 baseline model.

S_5 versus S_6 versus baseline. The results for the S_5, S_6, and baseline configurations are shown in figure 11. The figure shows results similar to those of the other configurations investigated, with values of c_z for S_5 and S_6 at $-15° < \phi < 15°$ being much greater than those for the baseline. For $-15° < \phi < 15°$, the values of c_z for S_5 and S_6 are virtually identical. At $\phi = 0°$, c_z is about 2.7 times larger than the baseline value (0.8 versus 0.3). The TRDSC on S_6 appears to be effective in reducing c_z compared with those of S_5 and the baseline for $-45° < \phi < -25°$ and $25° < \phi < 55°$.

Compared with the baseline configuration (fig. 11(b)), configurations S_5 and S_6 have a lower c_y/ϕ for $-10° < \phi < 10°$. (See table II for values.) The magnitudes of c_y for configurations S_5 and S_6 are virtually identical for $-20° < \phi < 15°$, which indicates that the TRDSC on configuration S_6 has little or no aerodynamic effect in this range of ϕ. Compared with the baseline values, the values of c_y/ϕ for S_5 and S_6 in the linear range of ϕ are low (about 2.7 times lower than the baseline). Based on comparison with data in tables I and II, if these configurations were used in a helicopter fuselage design, the fuselage side-force and yawing-moment characteristics would be expected to be low compared with those of the tail-boom cross-sectional configurations on the UH-60 and UH-1 helicopters. The values of c_y/ϕ for S_5 and S_6 are, however, larger in magnitude than the values of c_y/ϕ for the AH-64.

S_7 versus S_8 versus baseline. The results for the S_7, S_8, and baseline configurations are presented in figure 12. Both S_7 and S_8 have a much larger c_z within $-20° < \phi < 20°$ than that of the baseline. At $\phi = 0°$, c_z for S_7 and S_8 are 2.5 to 3 times that of the baseline. (See table II.) The effect of the TRDSC on the results of S_8 at $-45° < \phi < -25°$ and $25° < \phi < 60°$ is of interest because c_z for S_8 is much lower than it is for S_7 and for the baseline. For $70° < \phi < 90°$, S_7 (without a TRDSC) has the lowest c_z and the baseline has the largest value. Because much of the operational time for a helicopter is at $-30° < \phi < 30°$ (equal to sideward flight speeds of about 0 to 20 knots), where c_z for configurations

S_7 and S_8 is 2.5 to 3 times that of the baseline configuration, the down-load penalty for S_7 and S_8 fuselage designs will be much greater than that of the baseline.

In the range of ϕ where the data are linear in figure 12(b) ($-10° < \phi < 10°$), configurations S_7 and S_8 have identical slopes (see values in table II), and this equality indicates that the TRDSC has no effect on c_y in this range of ϕ. The side-force and yawing-moment characteristics of S_7 and S_8 when included in a fuselage design will likely be low compared with those generated by the baseline and are on the same order as those of a circular tail boom with a TRDSC (AH-64). (See tables I and II.)

S_9 versus baseline. The results for configuration S_9 (narrow rectangular shape with a TRDSC) and the baseline results are given in figure 13. The c_z (fig. 13(a)) is higher for S_9 at $-10° < \phi < 10°$ and is about 2 times larger than that of the baseline at $\phi = 0°$. For $45° < \phi < 90°$, c_z for S_9 is about one-third the baseline value.

The value of c_y/ϕ for S_9 (fig. 13(b)) is about 60 percent greater than for the baseline at $-10° < \phi < 10°$. In fact, of the nine configurations investigated, S_9 results in the steepest slope. It should also be noted that the largest positive and negative values of c_y for S_9 are about twice as large as the corresponding values of c_y for the baseline configuration, and the margin continues throughout $-15° > \phi > 15°$. S_9 would be expected to have high side-force and yawing-moment characteristics compared with those of the baseline when incorporated in a helicopter fuselage design.

Effect of Side-Force Characteristics (c_y/ϕ and maximum c_y) on Tail-Rotor Power

Figure 14 presents a bar chart of c_y/ϕ for $-10° < \phi < 10°$ for configurations S_1 to S_9 and the baseline. The effects of the maximum value of c_y on tail-rotor power were then calculated for configurations S_1 to S_9 based on a UH-1–class (Bell 204B) helicopter and are presented with flight data from the 204B (ref. 6) in figure 15. The 204B helicopter was used as a baseline configuration in this case because of the type of flight data available.

The data represented in the summary bar chart (fig. 14) are taken from the linear portion of the slopes between $-10° < \phi < 10°$. Configurations S_1, S_2, and S_9 have slopes that are greater than that of the baseline and therefore, in crosswinds could be expected to yield higher side-force characteristics than the baseline configuration when used in a helicopter fuselage. Also, higher values of c_y/ϕ contribute to higher fuselage yawing moments, which in right crosswinds (positive ϕ) would increase the tail-rotor power required. In right crosswinds, the tail rotor normally thrusts to the right; therefore, a positive value of c_y will then assist in yaw control.

Calculations based on a right crosswind condition of an airspeed of 20 knots and wind coming from 60° to the right of the nose of a UH-1 class (Bell 204B) helicopter indicate that the tail-rotor power required to overcome the boom force when configurations S_1 to S_9 are used in the tail boom would vary from about 0.3 to 2.3 times the power required of the baseline Bell 204B (fig. 15). Data are available from both flight investigation (ref. 6) and wind-tunnel investigation (ref. 3) to use in the calculations. The calculations are based on the following rationale. If the maximum value of c_y for configuration S_9 (-3.0 at $\phi = 15°$, fig. 13(b)) is compared with the corresponding value for the UH-1 tail-boom model (-1.3 with TRDSC, ref. 3), an estimate of the tail-rotor power needed to overcome the boom force can be made. The size and shape of the UH-1 and 204B tail booms are identical. The maximum measured c_y for the UH-1 model is assumed to represent the maximum boom contribution to tail-rotor power required (20 hp for full-scale helicopter for these conditions, ref. 6). When the maximum c_y for configuration S_9 is divided by the maximum value of c_y for the UH-1, the result is $3.0/1.3 = 2.3$; therefore, the maximum tail-boom contribution to tail-rotor power required for configuration S_9 is approximately 2.3×20 hp $= 46$ hp if configuration S_9 is installed as the boom shape on a UH-1–class helicopter. In terms of overall power, if the helicopter is assumed to require 600 hp to hover in a 20-knot wind, the change in tail-rotor power of 26 hp (46 hp $-$ 20 hp $=$ 26 hp) for the helicopter with an S_9-configured boom compared with the baseline represents an increase of 4.3 percent. It must be remembered for these calculations that two-dimensional data are being applied with three-dimensional data, so the results shown in figure 15 indicate trends only.

Effect of Down-Load Characteristics (c_z at $\phi = 0°$) on Main-Rotor Power

A summary bar chart that presents the section normal-force (down-load) coefficients c_z at $\phi = 0°$ for configurations S_1 to S_9 with those for the baseline configuration is given in figure 16. The down loads of all the polygon-shaped configurations are much higher than that of the oval-shaped baseline model because of the flat surfaces normal to the flow and

the increased surface area. With the same assumptions as given previously, the effects on main-rotor thrust of tail-boom down load in hover are computed and the results are presented in figure 17. If the polygon-shaped models are substituted for the baseline UH-60 tail boom, the calculated increase in hover down load on the boom would require an additional main-rotor thrust of approximately 1 to 2.5 percent. Again, the assumptions included in the calculations make the accuracy of the derived values questionable; however, the trends are believed to be applicable.

Concluding Remarks

An investigation was conducted in the Langley 14- by 22-Foot Subsonic Tunnel to determine the aerodynamic characteristics of nine large-scale two-dimensional polygon-shaped fuselage models that were nominally triangular (configurations S_1, S_2, S_5, and S_6), diamond (configurations S_3, S_4, S_7, and S_8), and rectangular (configuration S_9) in shape. Section side-force coefficients c_y and normal-force coefficients c_z were obtained on each model at angles of incidence ϕ from $-45°$ to $90°$ and compared with results from a UH-60 tail-boom cross-sectional model that served as the baseline configuration. Two-dimensional data from AH-64 and UH-1 tail-boom models were also used for comparison. Calculations were performed to obtain an approximation of effects of side-load and down-load characteristics of the polygon-shaped models on main- and tail-rotor thrust and power compared with those of a baseline. Based on analyses of results from this investigation, the following observations can be made:

1. The general trends of c_z and c_y as a function of ϕ for the nine polygon-shaped models were similar to the characteristic trend of the UH-60 baseline model data; however, there were important differences in magnitude.

2. Within $-15° < \phi < 15°$, values of c_z for S_1 to S_9 were larger than that for the UH-60 baseline model. At $\phi = 0°$, values of c_z for S_3 and S_4 were the largest of the nine configurations at about 3.5 times the baseline value. Configuration S_9 had the lowest value at about 2 times the baseline value.

3. The calculated increase in fuselage down load for the nine polygon-shaped configurations varied from 1.0 to 2.5 percent of main-rotor thrust compared with the UH-60 baseline.

4. Configurations S_1, S_2, and S_9 yielded greater slopes of c_y/ϕ at $-10° < \phi < 10°$ than the UH-60 baseline. Steeper slopes of c_y/ϕ and higher positive and negative values of c_y result in fuselage designs that are likely to produce higher side-force and yawing-moment characteristics than the baseline.

5. Configurations S_3 to S_8 had lower slopes of c_y/ϕ compared with the baseline within $-10° < \phi < 10°$. The values were closer to the value of a circular cylinder with a tail-rotor drive-shaft cover. Compared with the baseline, configurations S_3 to S_8 will result in moderate to low side-force and yawing-moment characteristics when incorporated into a helicopter fuselage design.

6. Calculations based on the maximum value of c_y for S_1 to S_9 indicate that the tail-rotor power required to overcome the tail-boom side force varied from about 0.3 to 2.3 times the baseline (Bell 204B helicopter) value.

NASA Langley Research Center
Hampton, VA 23681
June 25, 1992

References

1. Blake, Bruce; Hodder, David St. J.; and Hanker, Edward J., Jr.: *Wind Tunnel Investigation Into the Directional Control Characteristics of an OH-58A Helicopter.* USAAVRADCOM TR-83-D-18, U.S. Army, June 1984. (Available from DTIC as AD B084 796L.)

2. Brocklehurst, Alan: A Significant Improvement to the Low Speed Yaw Control of the Sea King Using a Tail Boom Strake. *Eleventh European Rotorcraft Forum*, City Univ. (London, England), 1985, pp. 32-1–32-11.

3. Wilson, John C.; and Kelley, Henry L.: *Aerodynamic Characteristics of Several Current Helicopter Tail Boom Cross Sections Including the Effect of Spoilers.* NASA TP-2506, AVSCOM TR 85-B-3, 1986.

4. Lockwood, Roy A.; Kelly, William A.; and Cason, Randall W.: *Flight Characteristics Test of the UH-60A With Tail Boom Mounted Strake.* USAAEFA Proj. No. 85-07, U.S. Army, Oct. 1986.

5. Wilson, John C.; Kelley, Henry L.; Donahue, Cynthia C.; and Yenni, Kenneth R.: *Developments in Helicopter Tail Boom Strake Applications in the United States.* NASA TM-101496, AVSCOM TM-88-B-014, 1988.

6. Kelley, Henry L.; Crowell, Cynthia A.; Yenni, Kenneth R.; and Lance, Michael B.: Flight Investigation of the Effect of Tail Boom Strakes on Helicopter Directional Control. *AHS 46th Annual Forum and Technology Display*, American Helicopter Soc., 1990, pp. 1161–1174.

7. Crowell, Cynthia A.; and Kelley, Henry L.: *Aerodynamic Effect of Strakes on Two-Dimensional Tail Boom Models of OH-58A and OH-58D Helicopters.* NASA TM-4248, AVSCOM TR-90-B-010, 1990.

8. Gentry, Garl L., Jr.; Quinto, P. Frank; Gatlin, Gregory M.; and Applin, Zachary T.: *The Langley 14-*

by 22-Foot Subsonic Tunnel: Description, Flow Characteristics, and Guide for Users. NASA TP-3008, 1990.

9. Rae, William H., Jr.; and Pope, Alan: *Low-Speed Wind Tunnel Testing*, Second ed. John Wiley & Sons, Inc., c.1984.

10. Polhamus, Edward C.: *Effect of Flow Incidence and Reynolds Number on Low-Speed Aerodynamic Characteristics of Several Noncircular Cylinders With Applications to Directional Stability and Spinning.* NASA TR R-29, 1959. (Supersedes NACA TN 4176.)

11. Polhamus, Edward C.; Geller, Edward W.; and Grunwald, Kalman J.: *Pressure and Force Characteristics of Noncircular Cylinders as Affected by Reynolds Number With a Method Included for Determining the Potential Flow About Arbitrary Shapes.* NASA TR R-46, 1959.

12. Lockwood, Vernard E.; and McKinney, Linwood W.: *Effect of Reynolds Number on the Force and Pressure Distribution Characteristics of a Two-Dimensional Lifting Circular Cylinder.* NASA TN D-455, 1960.

13. Taylor, P.: A Method of Predicting Fuselage Loads in Hover. *Seventh European Rotorcraft and Powered Lift Aircraft Forum*, Deutsche Gesellschaft fur Luft- und Raumfahrt e.v., Sept. 1981, Paper No. 49.

14. Achenbach, E.; and Heinecke, E.: On Vortex Shedding From Smooth and Rough Cylinders in the Range of Reynolds Numbers 6×10^3 to 5×10^6. *J. Fluid Mech.*, vol. 109, Aug. 1981, pp. 239–251.

15. Fage, A.; and Warsap, J. H.: *The Effects of Turbulence and Surface Roughness on the Drag of a Circular Cylinder.* R. & M. No. 1283, British Aeronautical Research Council, 1930.

Table I. Key Values of c_z and c_y for Tail-Boom Cross-Sectional Models of Baseline (UH-60), UH-1, and AH-64 Helicopters

[From ref. 3]

Configuration	c_z at $\phi = 0°$	Average c_y/ϕ at $-10° < \phi < 10°$, per degree
Baseline with TRDSC	0.30	−0.130
UH-1 with TRDSC	0.37	−0.110
AH-64 with TRDSC	0.61	−0.032
AH-64 without TRDSC (circular cylinder)	.65	−.010

Table II. Key Values of c_z and c_y for Configurations S_1 to S_9 and Baseline

Configuration	c_z at $\phi = 0°$	Average c_y/ϕ at $-10° < \phi < 10°$, per degree
S_1	0.91	−0.171
S_2 [a]	.97	−.182
S_3	1.08	−0.017
S_4 [a]	1.08	−.031
S_5	0.79	−0.049
S_6 [a]	.80	−.049
S_7	0.87	−0.031
S_8 [a]	.80	−.031
S_9 [a]	0.62	−0.207
Baseline (UH-60)[a]	.30	−.130

[a] Configuration with TRDSC.

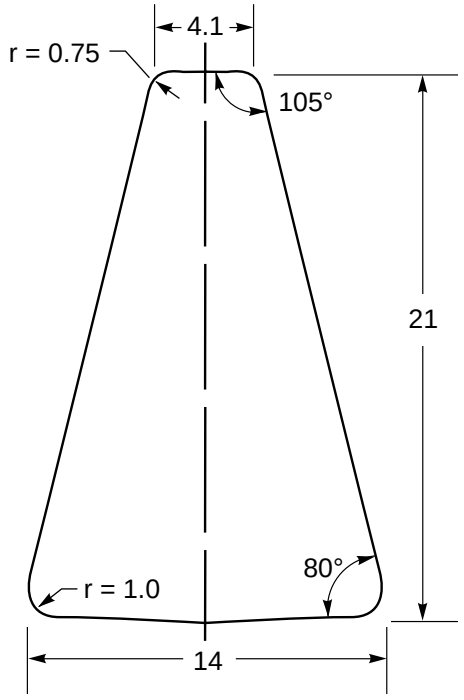

(a) S_1.

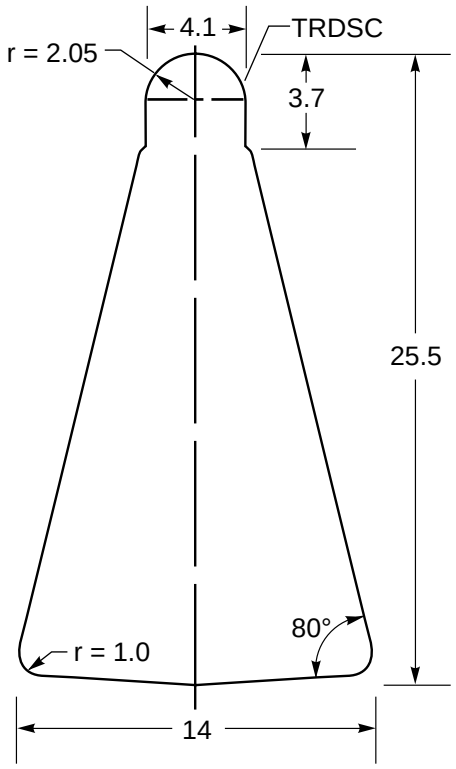

(b) S_2.

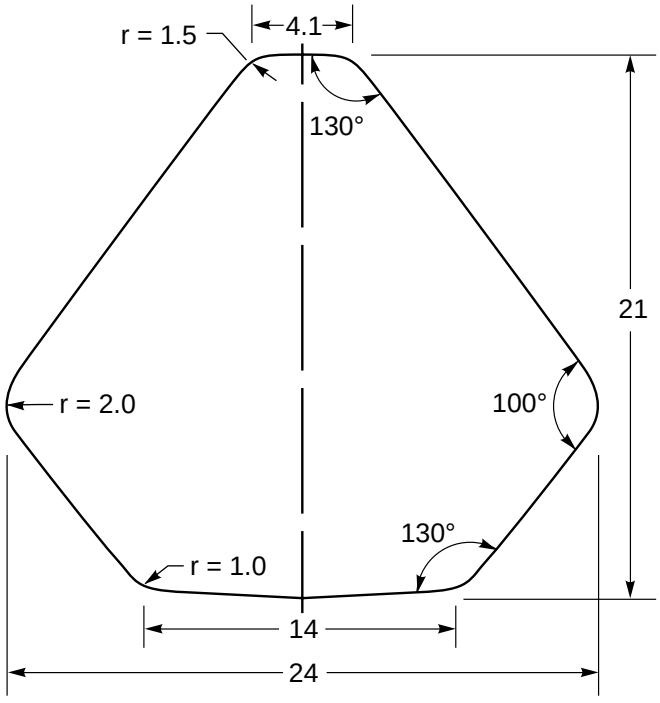

(c) S_3.

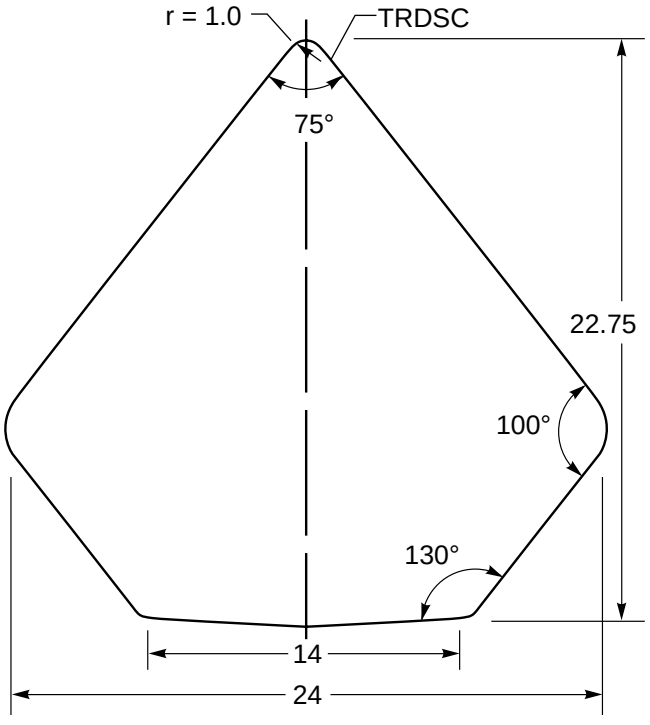

(d) S_4.

Figure 1. Models of polygon-shaped fuselage cross sections. All linear dimensions are in inches.

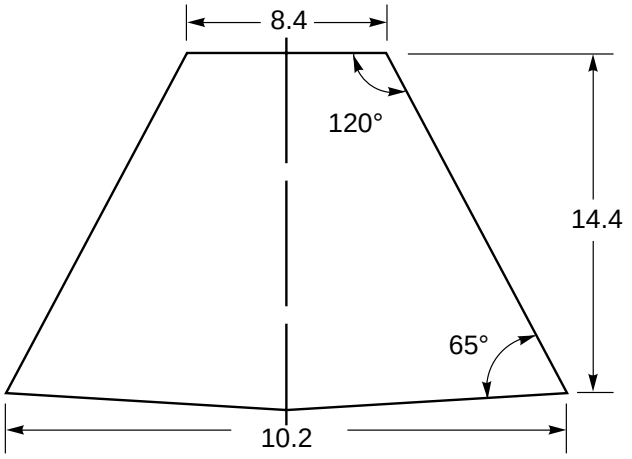

(e) S_5.

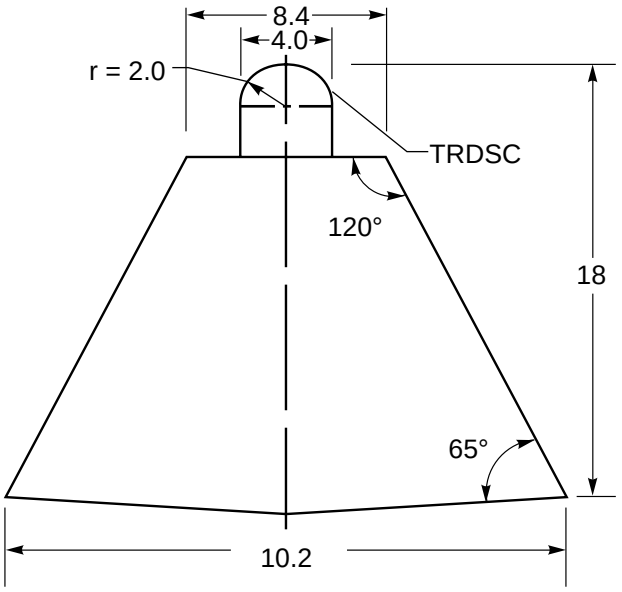

(f) S_6.

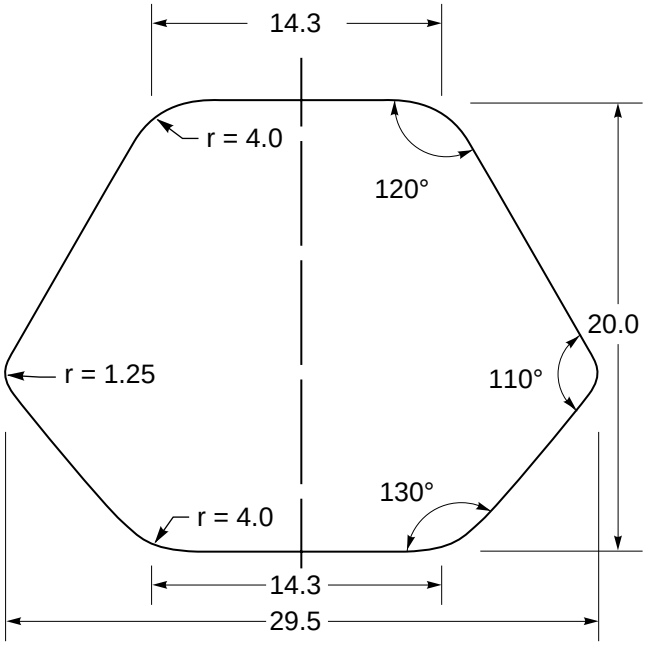

(g) S_7.

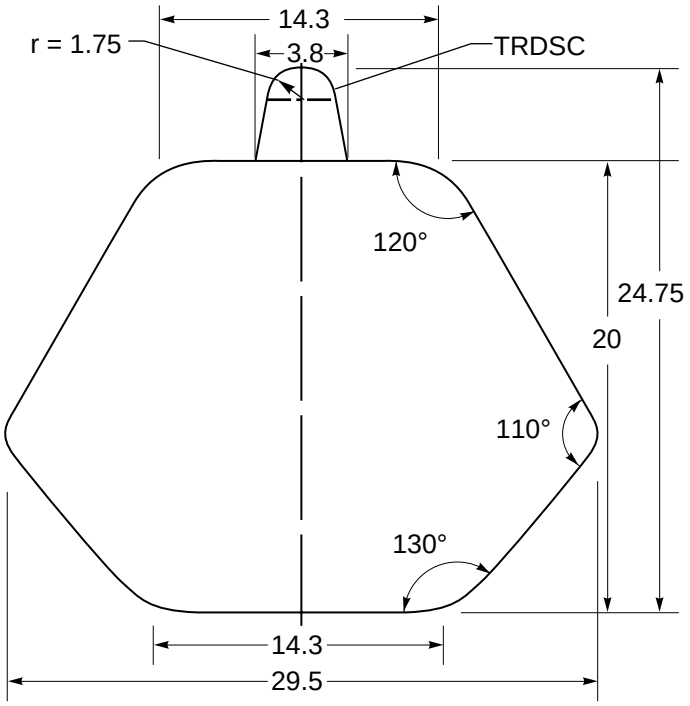

(h) S_8.

Figure 1. Continued.

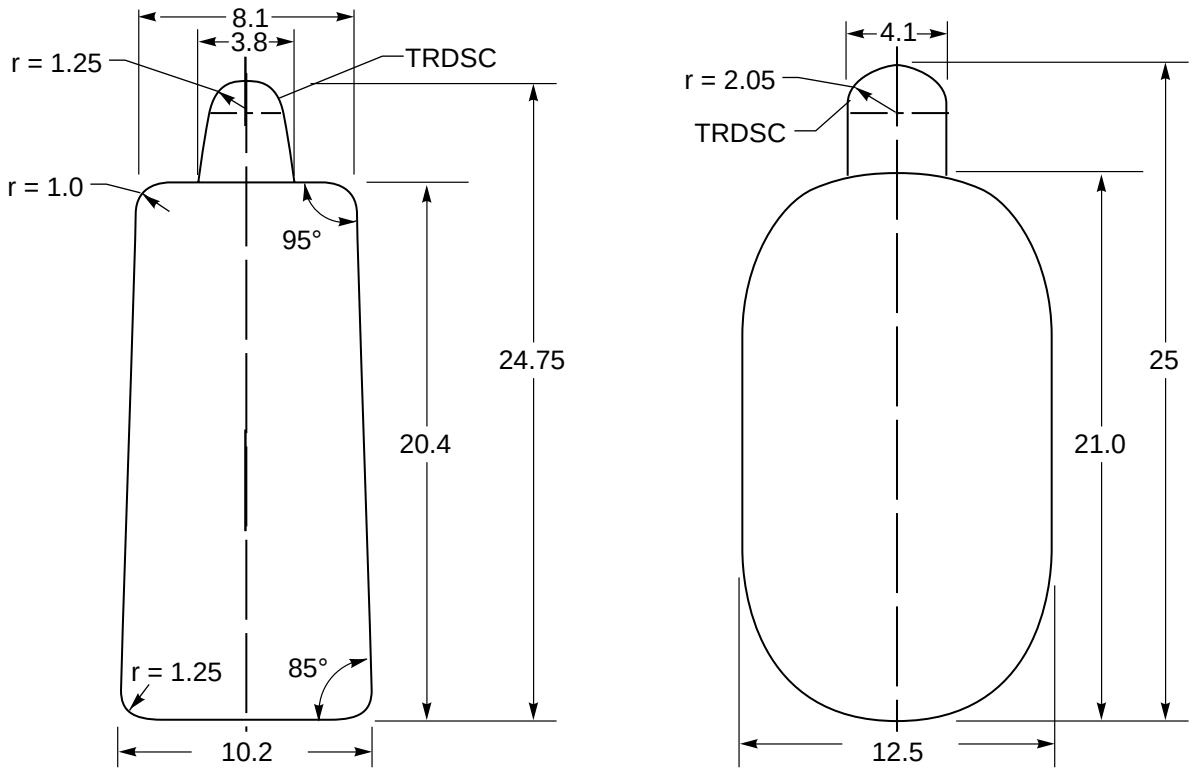

(i) S_9.

(j) Baseline (UH-60 tail-boom model).

Figure 1. Concluded.

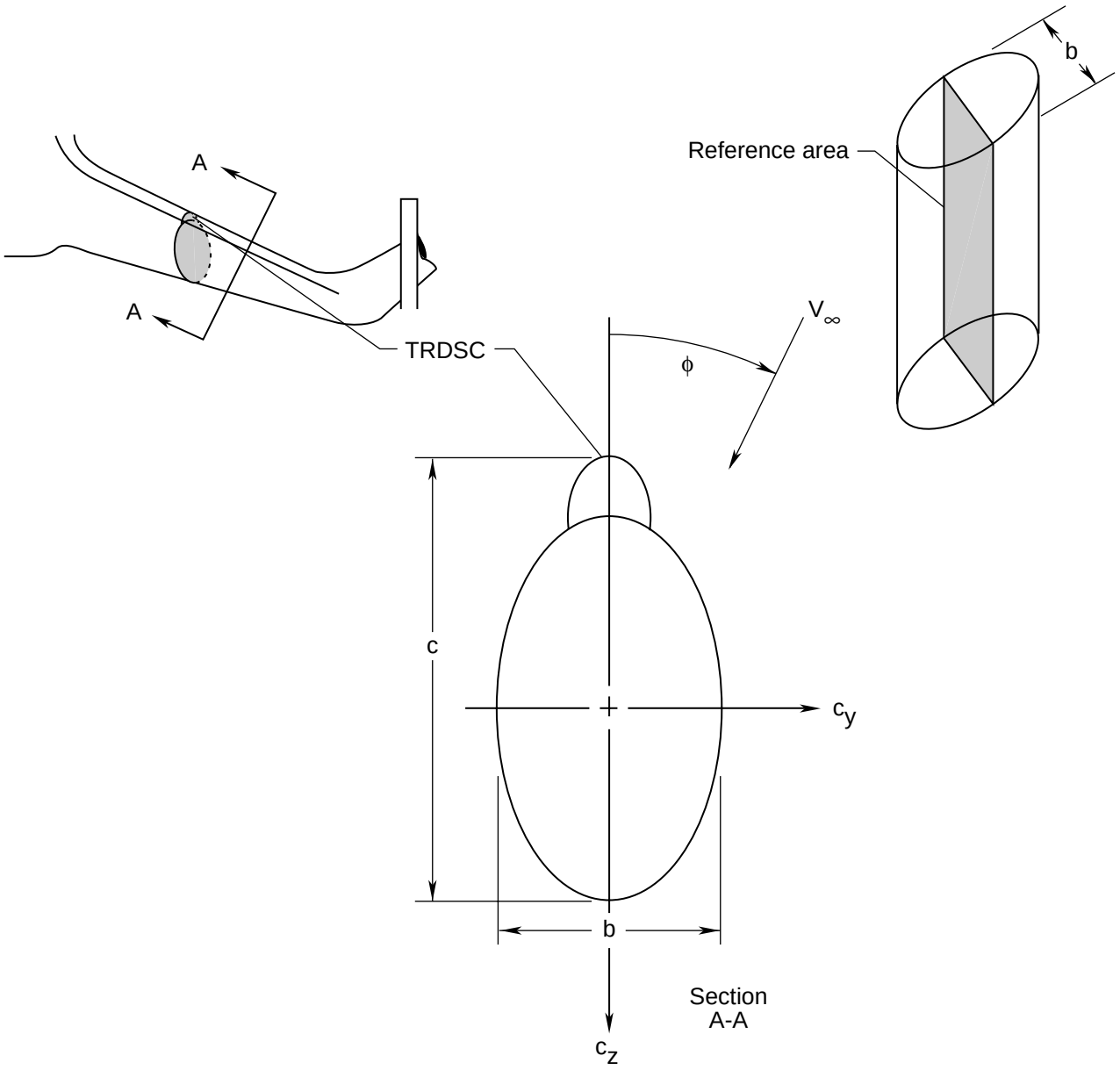

Figure 2. Conventions for positive sense of flow inclination, model reference dimensions, and aerodynamic coefficients.

Figure 3

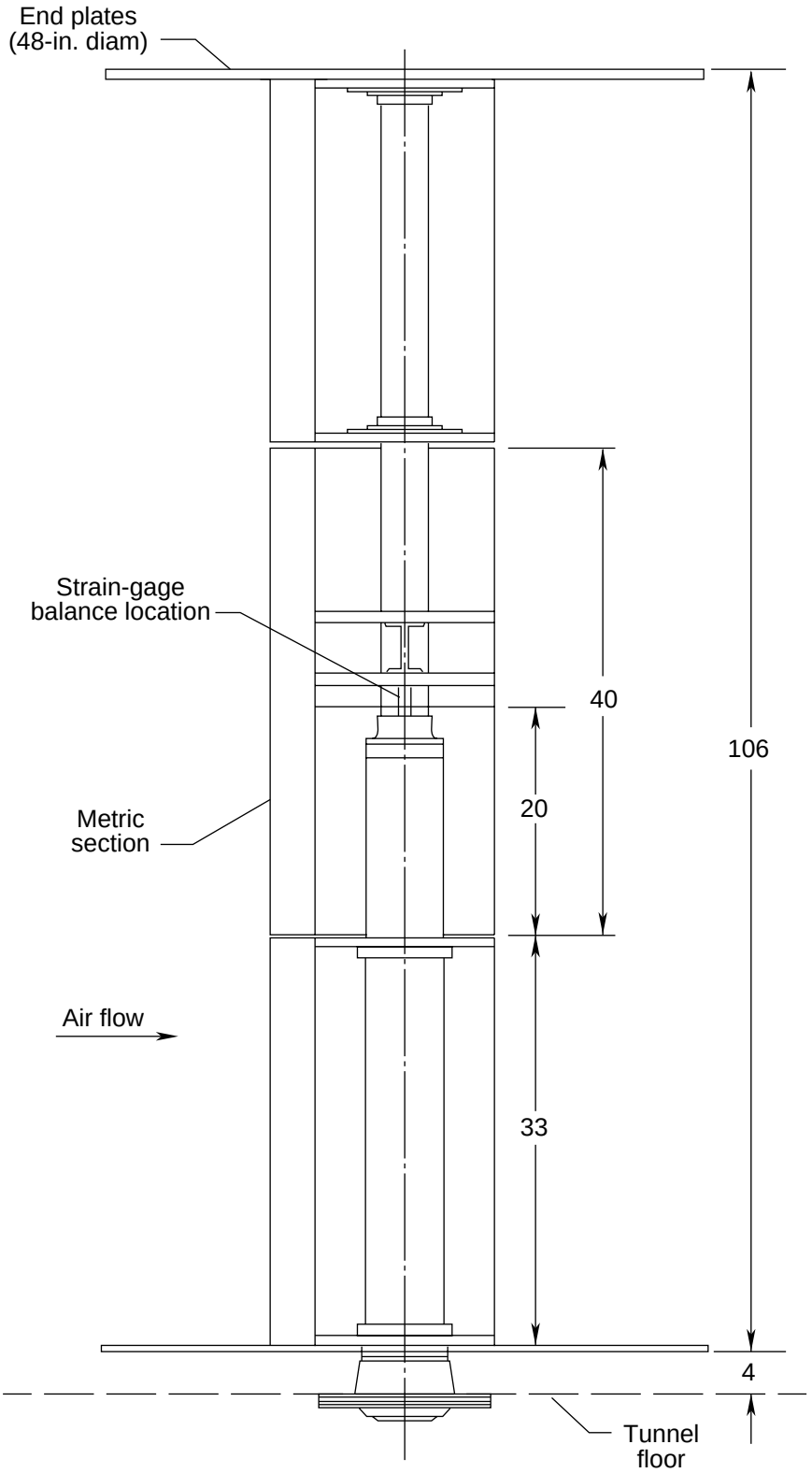

Figure 4. Helicopter cross-sectional test apparatus. All linear dimensions are in inches.

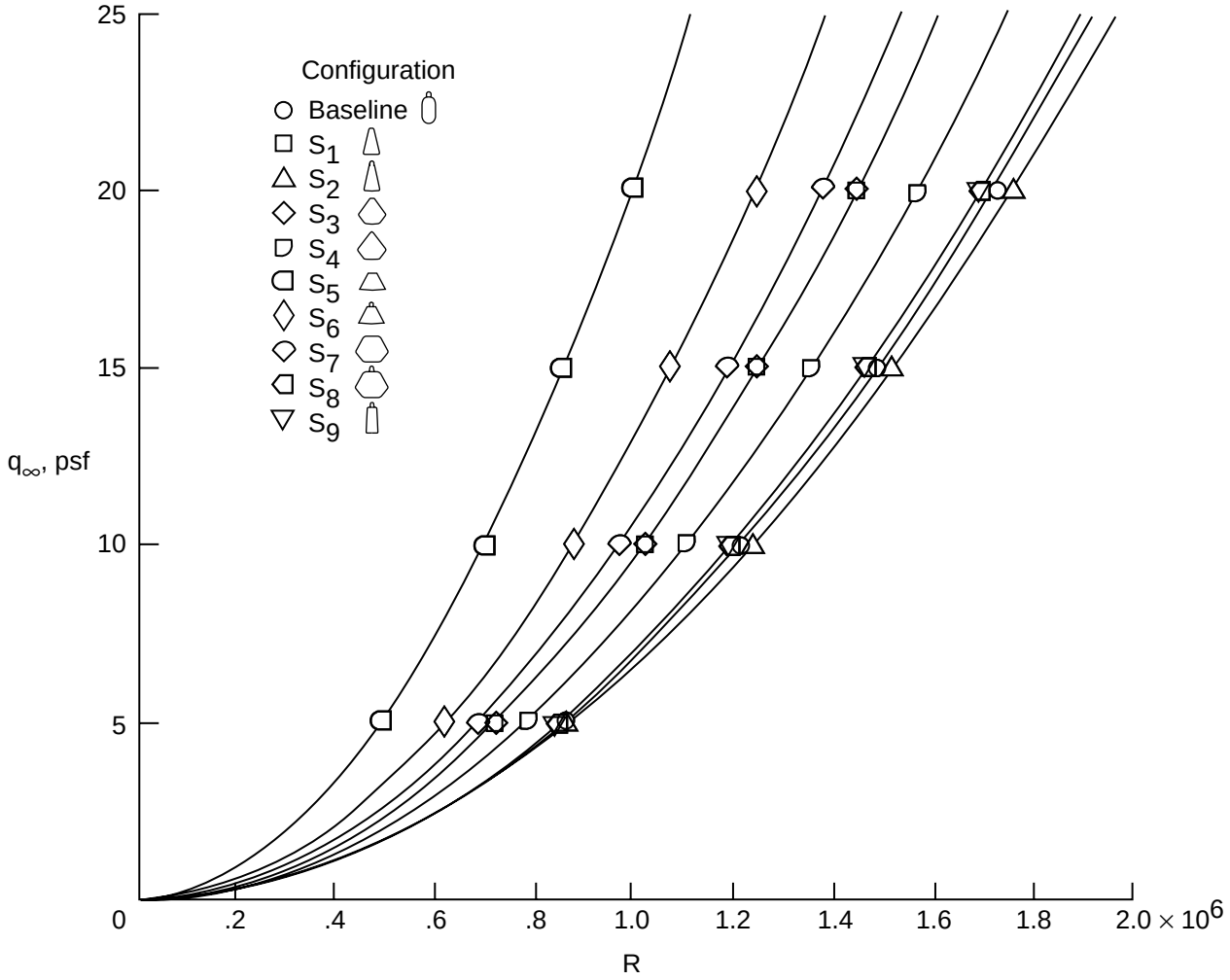

Figure 5. Variation of model Reynolds number with tunnel free-stream dynamic pressure.

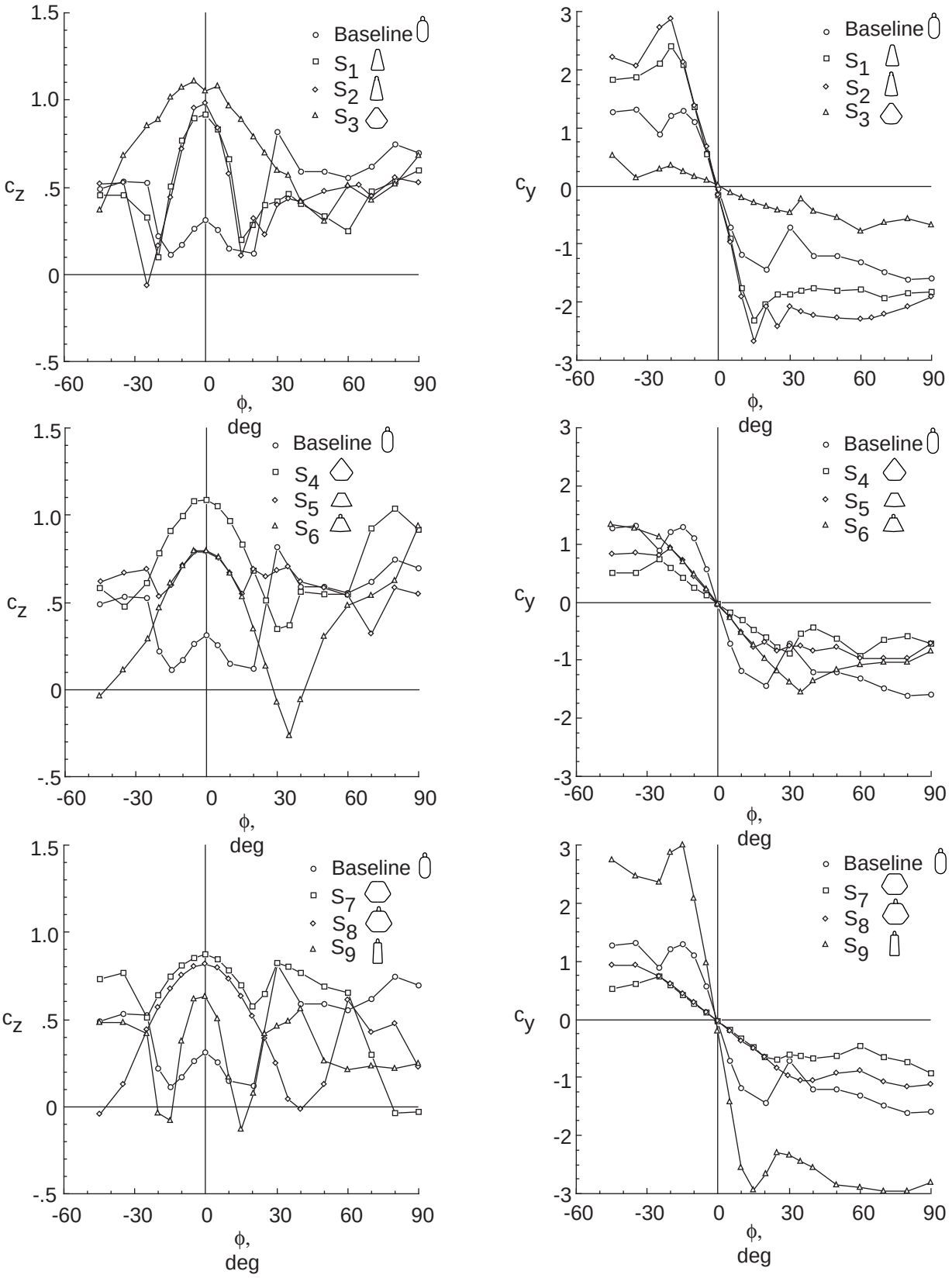

(a) Normal-force coefficient.

(b) Side-force coefficient.

Figure 6. Aerodynamic characteristics of configurations S_1 to S_9 and baseline.

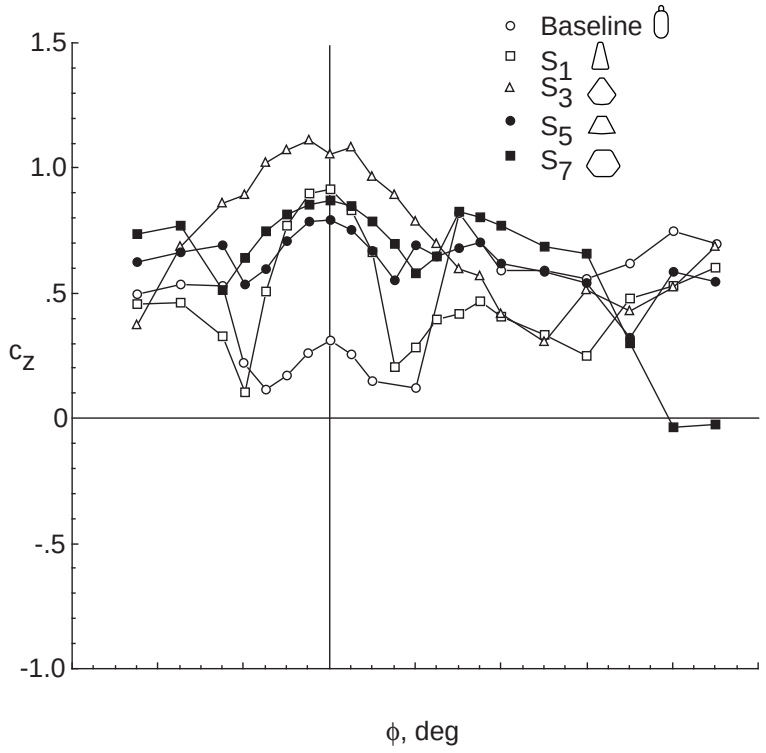

(a) Normal-force coefficient.

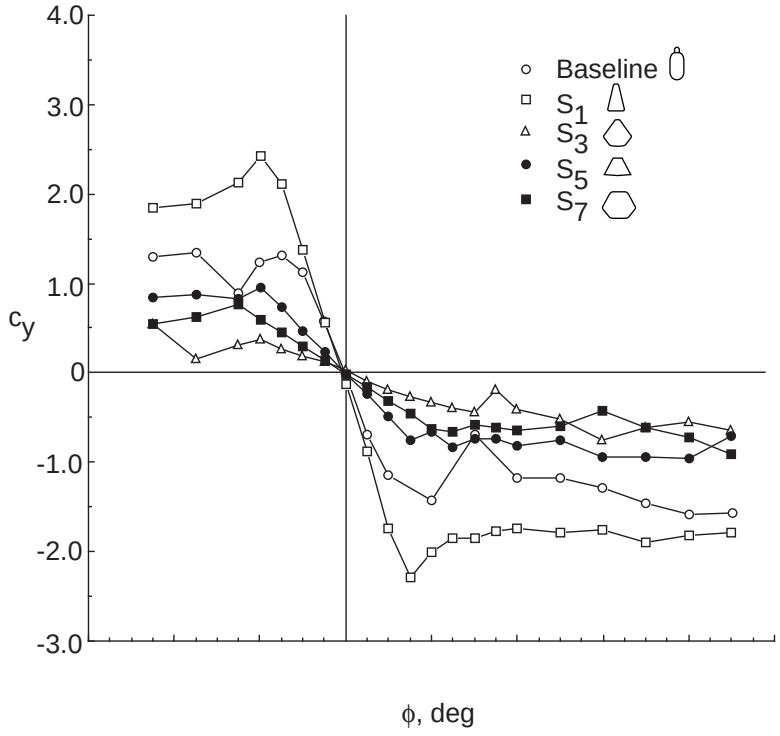

(b) Side-force coefficient.

Figure 7. Aerodynamic characteristics of configurations S_1, S_3, S_5, S_7 (without TRDSC), and baseline.

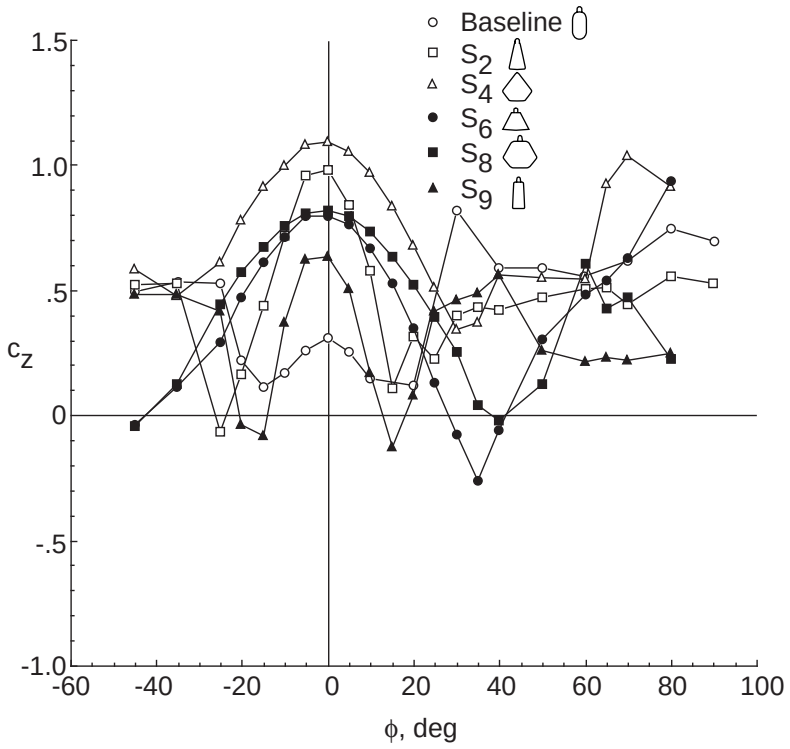

(a) Normal-force coefficient.

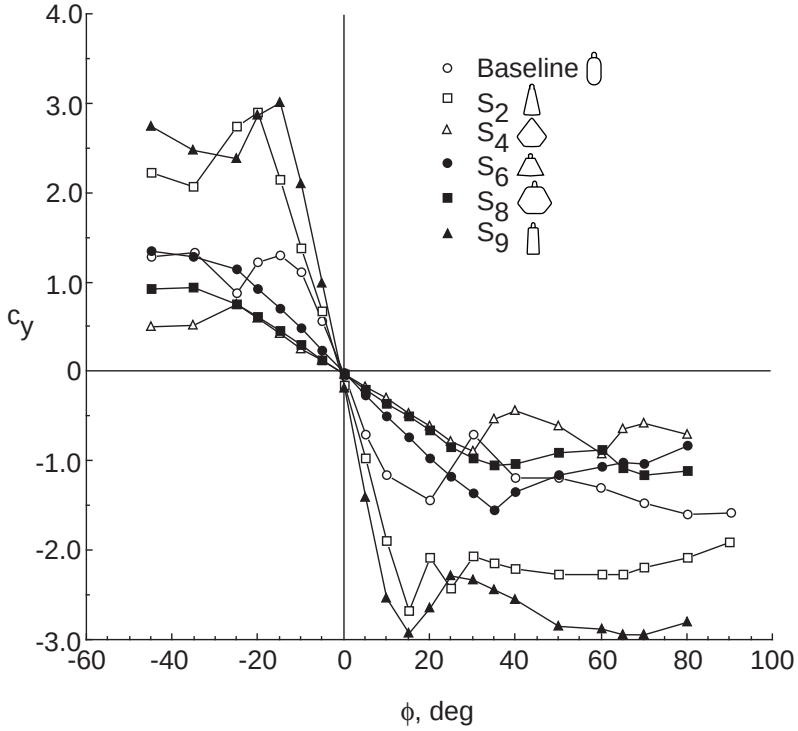

(b) Side-force coefficient.

Figure 8. Aerodynamic characteristics of configurations S_2, S_4, S_6, S_8, S_9 (with TRDSC), and baseline.

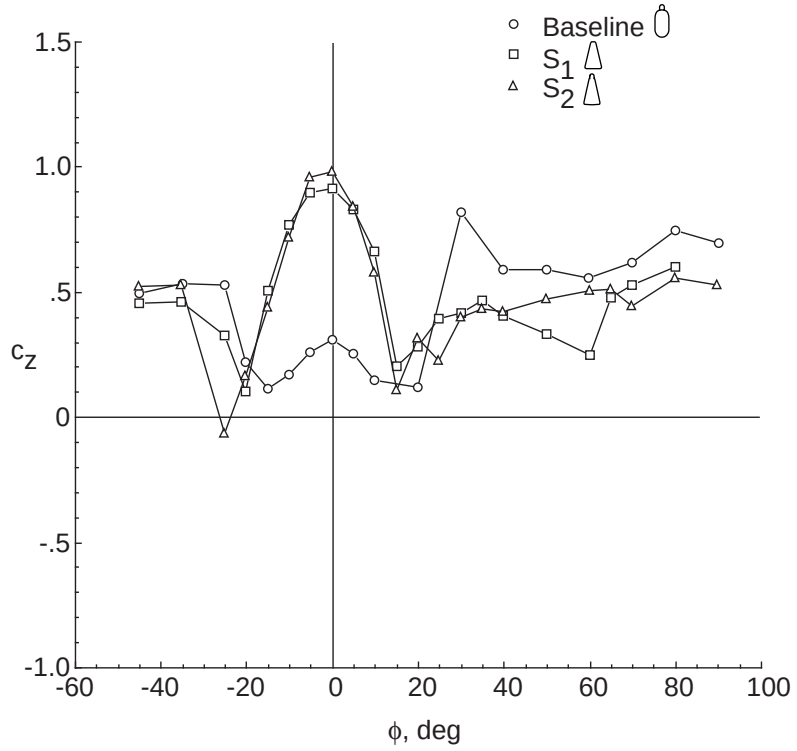

(a) Normal-force coefficient.

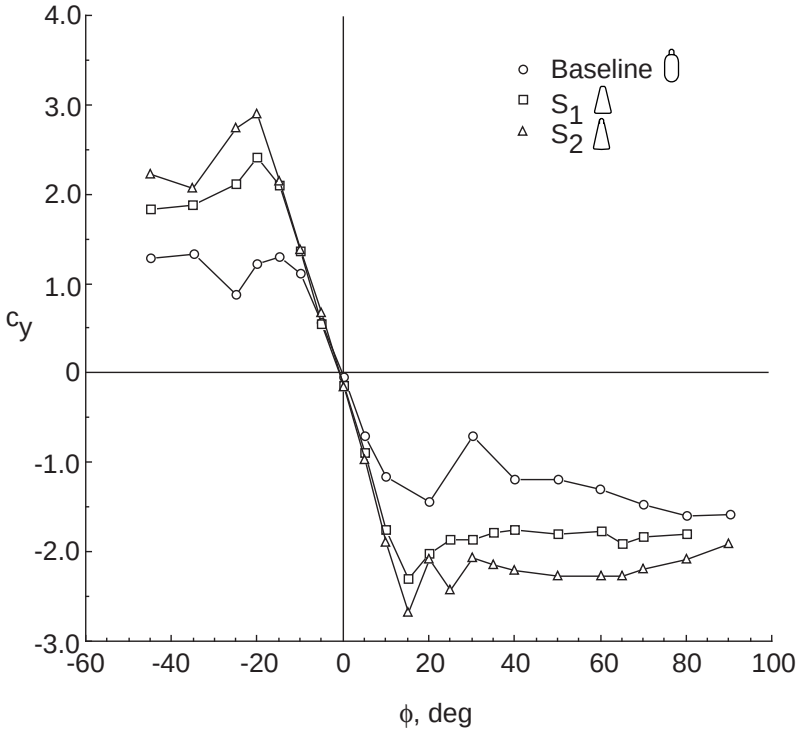

(b) Side-force coefficient.

Figure 9. Aerodynamic characteristics of configurations S_1, S_2, and baseline.

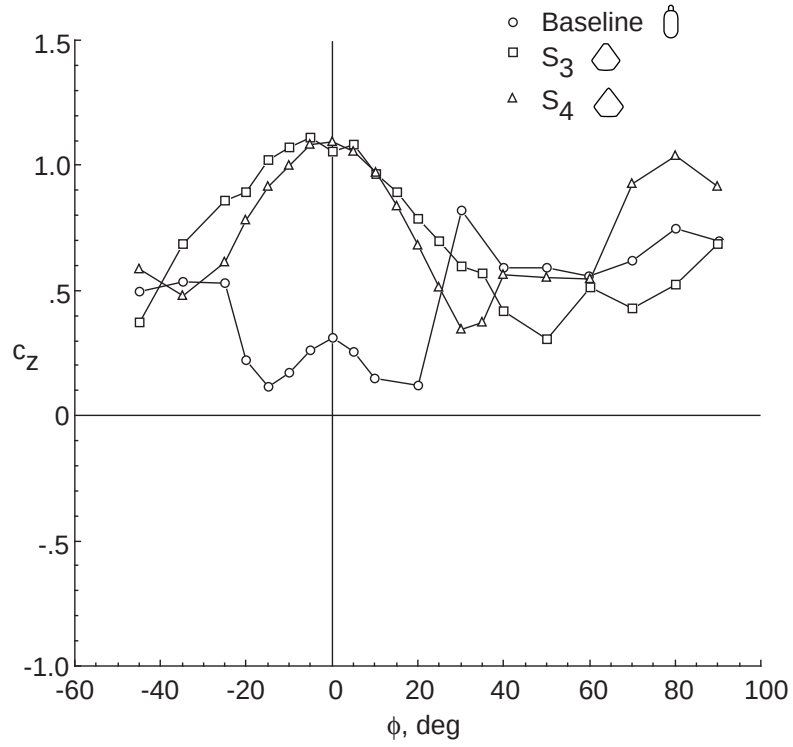

(a) Normal-force coefficient.

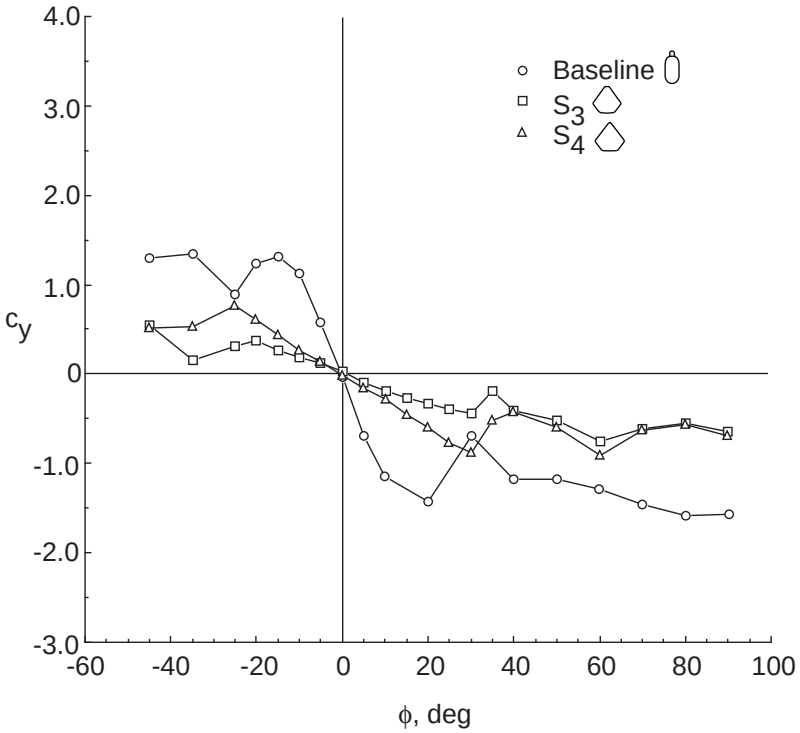

(b) Side-force coefficient.

Figure 10. Aerodynamic characteristics of configurations S_3, S_4, and baseline.

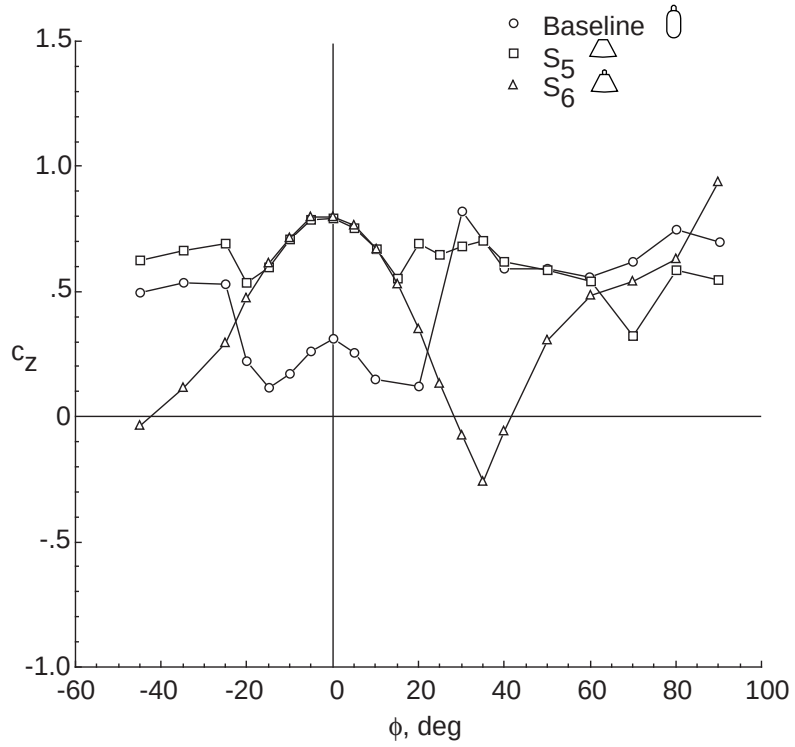

(a) Normal-force coefficient.

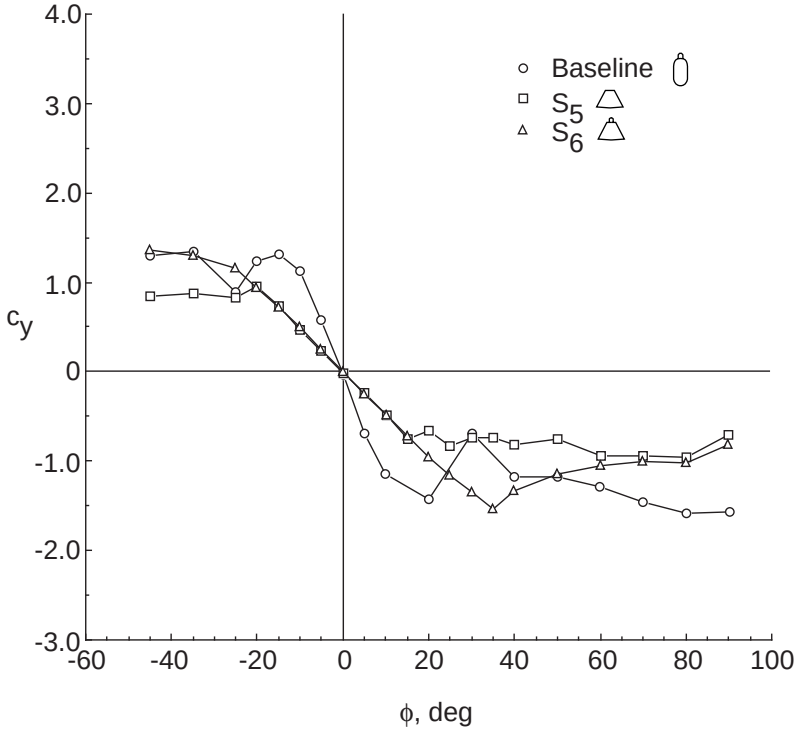

(b) Side-force coefficient.

Figure 11. Aerodynamic characteristics of configurations S_5, S_6, and baseline.

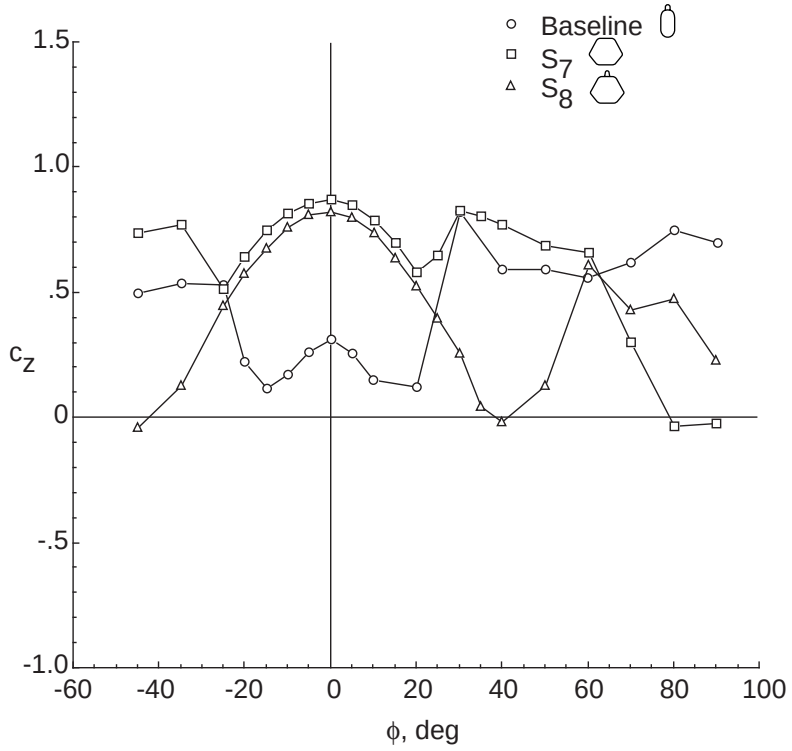

(a) Normal-force coefficient.

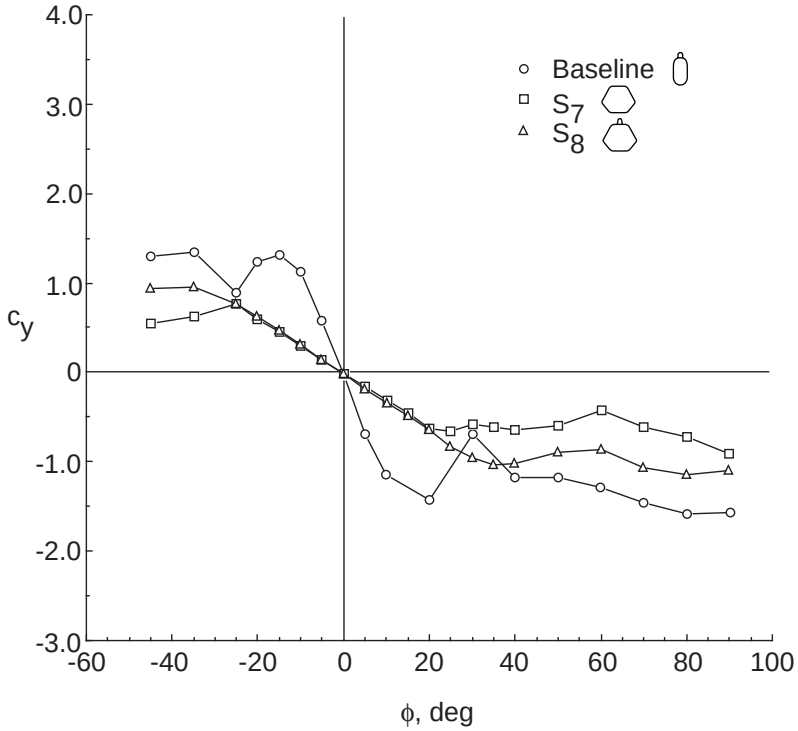

(b) Side-force coefficient.

Figure 12. Aerodynamic characteristics of configurations S_7, S_8, and baseline.

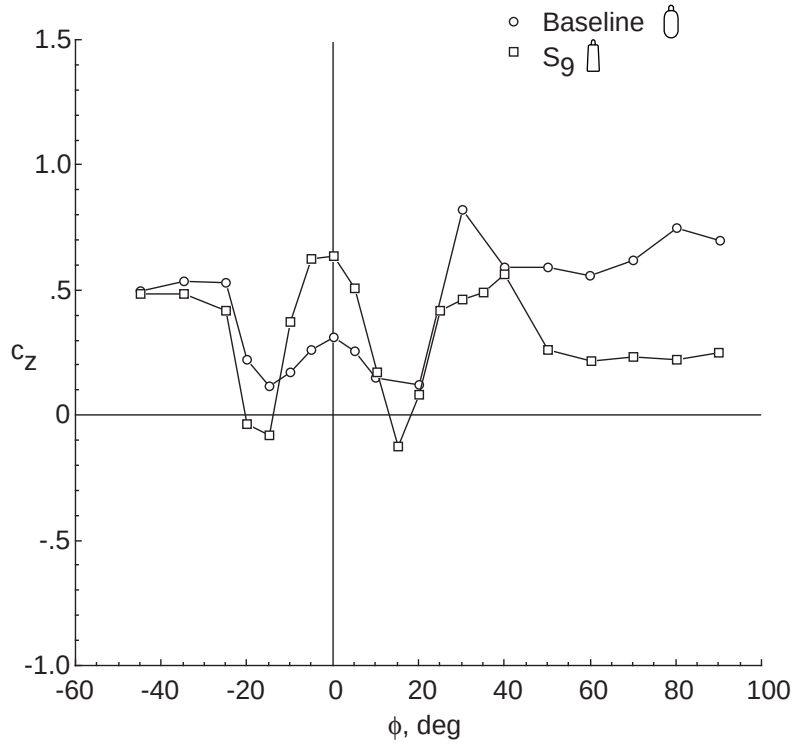

(a) Normal-force coefficient.

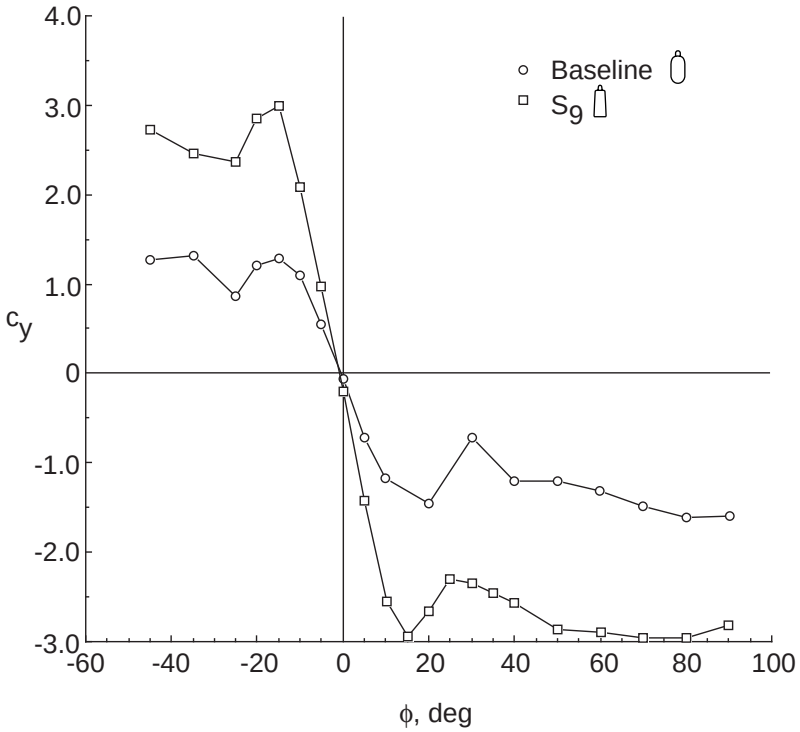

(b) Side-force coefficient.

Figure 13. Aerodynamic characteristics of configurations S_9 and baseline.

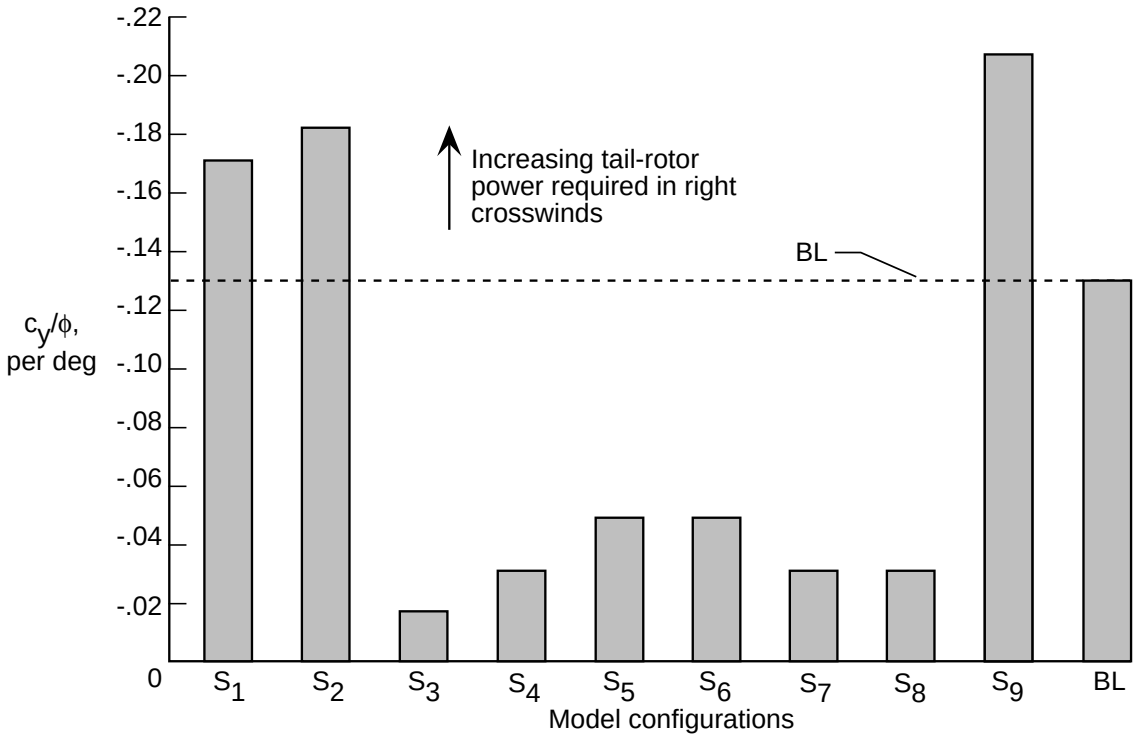

Figure 14. Slope c_y/ϕ in linear range of data ($-10° < \phi < 10°$) for configurations S_1 to S_9 and baseline model (UH-60).

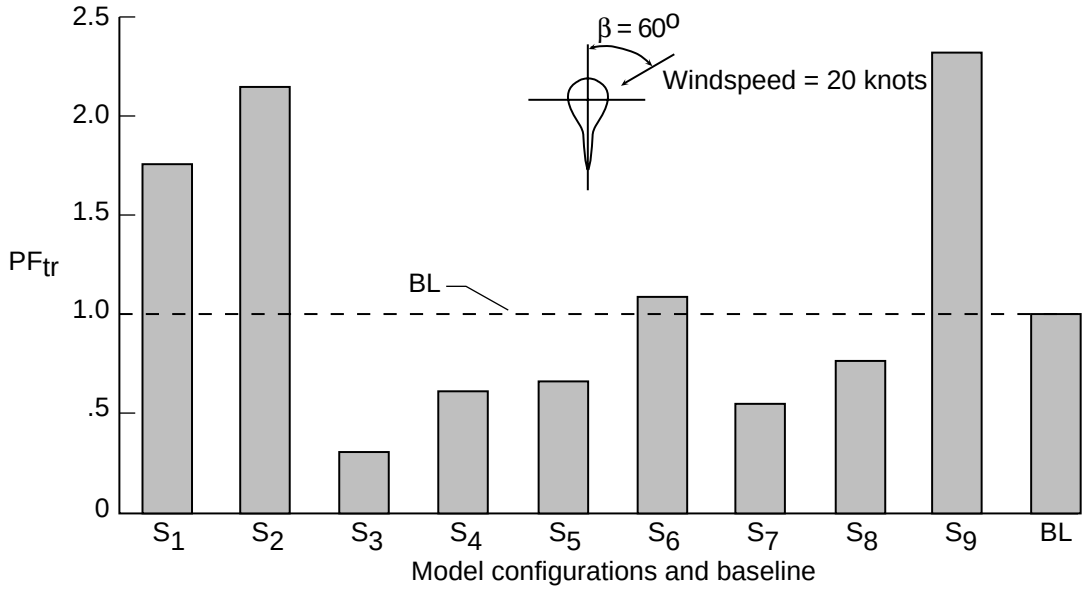

Figure 15. Tail-rotor power factor calculated from data for maximum c_y for configurations S_1 to S_9 and baseline helicopter (Bell 204B).

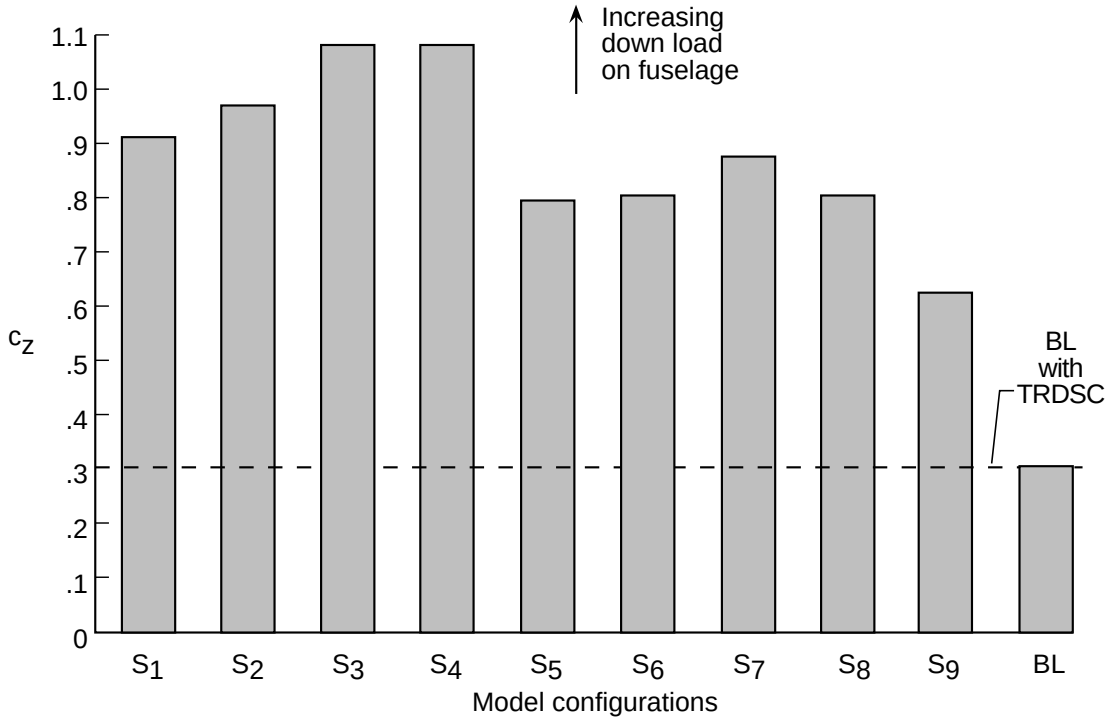

Figure 16. Value of c_z at $\phi = 0°$ for configurations S_1 to S_9 and baseline model (UH-60).

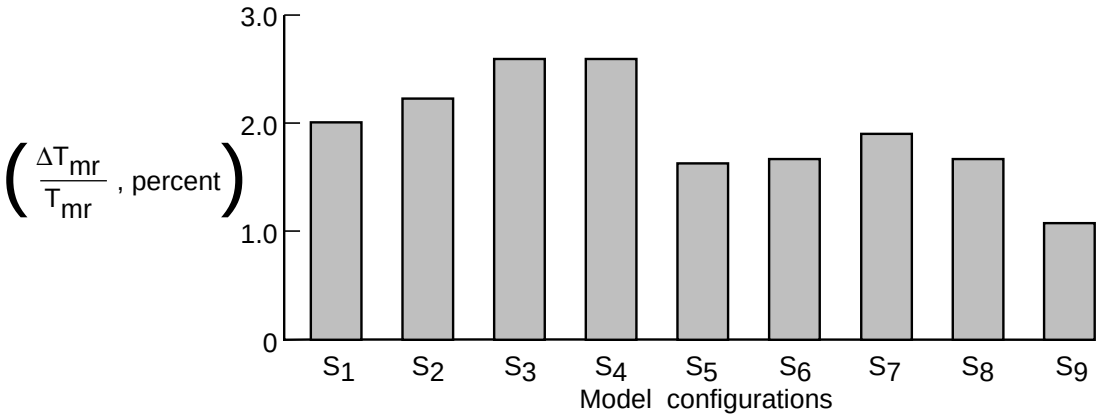

Figure 17. Effect of c_z at $\phi = 0°$ on $\Delta T_{\mathrm{mr}}/T_{\mathrm{mr}}$ in hover for configurations S_1 to S_9 relative to baseline model (UH-60).